ORIGINAL PAPER

Fourier–Voronoi-based generation of realistic samples for discrete modelling of granular materials

Guilhem Mollon · Jidong Zhao

Abstract This paper presents a novel method to generate realistic packings for discrete modelling of granular materials. To generate a packing of 2D dense sample in a container of arbitrary shape, a number of key particle properties are identified as the targeted ones to reproduce, including the grain size distribution, density, particles orientations as well as specific shape characteristics of the particles. Four descriptors, including elongation, circularity, roundness, regularity, are chosen to characterize the particle shape. The considered container is discretized by a Voronoi tessellation with prescribed cell size and orientation distributions. Each Voronoi cell is then filled with a particle with prescribed shape characteristics. Several algorithms are proposed and are compared in terms of their computational efficiency and accuracy to define the particle contours, to constrain the Voronoi tessellation and to fill the Voronoi cells with particles. Two examples are further employed to demonstrate the accuracy and the potential usefulness of the proposed method for a wide range of applications where discrete modelling of granular media is important.

Keywords Granular media · Particle packing · Particle shape · Voronoi tessellation · DEM

1 Introduction

The micromechanical behaviour of granular materials has drawn growing attention across a wide range of scientific and engineering fields, such as sedimentology, geomechanics,

G. Mollon (✉) · J. Zhao
Department of Civil and Environmental Engineering,
Hong Kong University of Science and Technology, Clearwater Bay,
Kowloon, Hong Kong
e-mail: guilhem.mollon@gmail.com

mining, chemical engineering, pharmaceutical and powder industries. While advanced experimental techniques enable us to observe the grain-scale behaviour of granular materials [1–3], modern computing power has led to unprecedented progresses towards numerical modelling of granular materials as discrete system, which provides us with much richer information and deeper insight into the microscopic behaviour of granular media that are not otherwise obtainable by experiments. The discrete elements method (DEM), pioneered by Cundall and Strack [4] and further developed by many others, is one of the prominent numerical tools of this kind.

One of the major challenges for DEM modellers today is how to accurately account for the complex shapes of real particles in the modelling. Natural sands, for example, may vary in shape, roundness, angularity, roughness and many other intrinsic properties, depending on their geological history and mineralogical composition [5,6]. These properties affect considerably the overall mechanical behaviour of these materials and need to be carefully considered in any discrete modelling of them in order for the simulation results to be reliable. While DEM has traditionally been based on idealized circular (2D) or spherical (3D) particles due obviously to their simplicity and computational efficiency, there have been studies to consider the shape effect of particles by using clusters (clumps) of discs/spheres [8–14], super-ellipsoids [15–17], pentagons [18], rounded-cap rectangles [19], polyarcs [20], cylinders [21], polyhedrons [22–29], or the so-called "potential particles" [30]. Using rolling resistance in conjunction with spherical particles has also been considered in some DEM studies as an equivalent way to account for irregular particle shape [7]. Limited success has been achieved by some of these studies to reproduce/predict the inherent phenomena relevant to granular materials (e.g. the fabric evolution and critical state of a sheared sand

[20] or energy dissipation in a rock avalanche [25,26]). These methods, however, remain to be too simplified to offer accurate description of the real shape of particles and hence serve at best as qualitative or phenomenological characterization of the influence of non-spherical particle shape. A systematic and comprehensive way to describe particle shape for discrete modelling is highly desirable but unavailable.

In addition to particle shape, how to properly pack particles with different size (and shape) to generate a realistic sample remains another unsolved issue. A packing method to generate particles in a container with a desired shape is generally subjected to a number of constraints, including the number of particles and their size distribution, the desired density (or void ratio) and the required orientation distribution. A conceptually straightforward way would be based on gravitational deposition, which attempts to reproduce the natural deposition process of granular materials. This method has the advantage to deal with complex particle shape, but in most cases can be extremely time-consuming. Moreover, it cannot be applied to arbitrary container shapes and is not able to reproduce certain desired properties, such as the target fabric anisotropy important to geomechanics study. Alternative to this deposition method are some geometric packing methods [31–33]. These methods appear to be very powerful for the packing of spherical particles, but may encounter great difficulties in dealing with particles of complex shapes. An interesting alternative approach was proposed in the pioneering work by Tilemans and Herrmann [27], in which a very dense packing is generated by discretizing a container domain into Voronoi cells [46] and then using each of these cells as a polygon-shaped particle. This method was then adapted and improved in [28,29], and each sharp polygon was replaced by sphero-polygons for more rigorous neighbourhood and contact detections.

This paper aims to develop a methodology to produce realistic packings of particles with complex particle shape for discrete modelling. Novel to the method are the constraints imposed to ensure that the generated particles and packings match quantitatively important statistical properties of the targeted real material, despite its seeming similarity in concept for the particle packing as in [27–29,46]. The formulation and description of the method will be presented for the two-dimensional case, and further discussion will be made on the generalization of the method to more realistic three-dimensional modelling. The method has been based on considerable improvements over some existing approaches [34–38] and features the following innovations:

(a)   Based on the spectral method proposed in [34–36], the main features of particle shape of a granular material will be characterized by the mean of a discrete spectrum which defines the irregularities of the shape. The specific spectrum for a granular material is chosen based on statistical data observed on real particles of the material [39].

(b)   A constrained Voronoi diagram will be defined to partition the container of the granular material into a number of "cells" (i.e. sub-domains of this container, defined by polygons). The number of cells should be equal to the number of particles composing the desired sample, and a method called Inverse Monte-Carlo (IMC, proposed in [37,38]) is used to constrain the Voronoi tessellation to match some targeted size and orientation distributions. This approach is analogous to the one of [27] and of [28,29], but with a better control over the cells statistics.

(c)   Each Voronoi cell will be filled with a particle with specified spectrum defined at Step 1 as well as a prescribed solid fraction. After the filling, a simple algorithm [40,41] will be used to replace each complex particle shape by an equivalent collection of overlapping discs [also called overlapping discrete element clusters (ODECs)] for future discrete modelling.

Upon finishing all three steps, the method is expected to produce a collection of particles with the correct shape properties (due to Step 1), the correct size and orientation distributions (due to the Voronoi diagram obtained by IMC in Step 2), and the desired void ratio/solid fraction (due to the filling process of Step 3). The three steps will be described in more detailed in Sects. 2, 3 and 4 of this article, followed by several demonstrative examples of the method as well as discussion on its accuracy and relevant issues to 3D generalization.

2 Generation of realistic particles

2.1 Shape descriptors

Describing the shape of a granular particle such as sand proves to be challenging. A variety of shape descriptors have been proposed in the literature (see a relatively complete review in [5]). The present study only focuses on 4 descriptors of shape, namely the elongation, the roundness, the circularity and the regularity (see Fig. 1). The elongation of a 2D particle (Fig. 1a) is defined by following the definition in [5]:

$$\text{Elongation} = S/L \qquad (1)$$

where S is the smallest possible dimension of a grain (obtained by minimization with respect to an angle of rotation θ, see Fig. 1a), and L is the dimension of the particle in the direction of θ (which may be slightly different from the longest dimension of the particle). The corresponding angle θ is a good descriptor of the orientation of the particle. The particle roundness employs the definition provided in [42]:
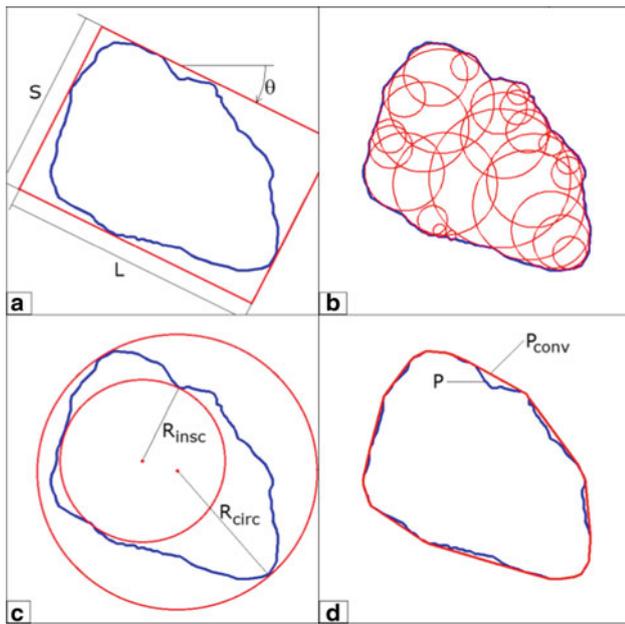
Fig. 1 Global shape descriptors of an illustrative particle: **a** elongation $= 0.663$ and $\theta = -29.7°$; **b** roundness $= 0.370$; **c** circularity $= 0.746$; **d** regularity $= 1.431$

$$\text{Roundness} = \frac{\sum R_c}{n_c \cdot R_{insc}} \qquad (2)$$

In the original definition in [42], R_{insc} is the radius of the largest inscribed circle in the particle, and the R_c terms correspond to the radii of the circles that approximate the corners of the particle contour (it thus implies that the n_c corners of the particle are represented by n_c circles of respective radii R_c). It is therefore a measure of the average sharpness of the angles of the particle. However, this definition is not perfectly objective since it is difficult to determine what curve along the contour of a particle is sharp enough to be called a "corner". To facilitate easy reproducibility for this shape descriptor, the original expression of Eq. (2) is slightly modified here. Specifically, the n_c circles considered here include all circles covering the entire contour of the particle, not only the ones used to approximate the corners of the particle (Fig. 1b). Note that the method used here to fill a 2D particle with circles was originally proposed in [40], which will be discussed in detail later. Besides the measure of the corners' sharpness, the circularity of a particle follows the definition in [43]:

$$\text{Circularity} = \sqrt{\frac{R_{insc}}{R_{circ}}} \qquad (3)$$

where R_{circ} is the circumscribed circle of the particle (see Fig. 1c). Roundness and circularity are somehow related, but circularity is believed to be a better description of the overall shape of a particle, irrespective of the sharpness of its angles. Furthermore, to describe the roughness of the parti-

cle surface, a so-called irregularity index has been defined in [5], but its implementation is difficult in practice. A new descriptor called regularity is proposed here:

$$\text{Regularity} = \log\left(\frac{P}{P - P_{conv}}\right) \qquad (4)$$

As shown in Fig. 1d, P is the perimeter and P_{conv} is the convex perimeter of the particle. Note that the contour of the particle has to be discretized by a number of points (for example, 500 in the present study) to represent its perimeter confidently. With the definition of Eq. (4), a perfectly convex particle (such as a circle, for example) therefore has an infinite regularity. However, due to round-off error in the floating-point algorithm used to compute the convex envelope, a regularity greater than 3 or 4 (corresponding to a relative difference between the perimeter and the convex perimeter smaller than 10^{-3} or 10^{-4}, respectively) is virtually equivalent to a perfect regularity. These four descriptors have been chosen among a large number of existing ones because they cover all the typical scales on the morphology of a particle. Elongation deals only with the very general shape, circularity concerns with the main irregularities of the contour, roundness addresses the sharpness of the angles, and regularity characterizes the surface roughness of the particle (a fifth scale would correspond to the contact friction introduced in the DEM code).

2.2 Fourier descriptors

There is an alternative approach proposed in [44] based on the discrete Fourier transform (DFT) of the contour of the grain which has been used extensively [34,36]. In the 2D case, a suitable centre O for the particle is chosen. The contour of the grain is then discretized by N_P points P_i separated by a constant angle θ_P with respect to O (i.e. such that $\theta_p = 2\pi/N_p$). Thus, each point P_i is defined by an angle θ_i and a radial distance $r_i = OP_i$. Following the Fourier theory, the discrete signal $r_i(\theta_i)$ can be represented by the following series:

$$r_i(\theta_i) = r_0 + \sum_{n=1}^{N}[A_n \cos(n\theta) + B_n \sin(n\theta)] \qquad (5)$$

where n is the harmonic number and N is the total number of harmonics. As stated in [35], this method is only suitable for a certain class of particle shapes, namely the "star-like" particles. More precisely, a particle may be described by this method if there exists a suitable point O inside the particle contour, such that all the half-lines arising from O cross the particle contour exactly one time. This drawback has actually a limited effect, since a majority of the natural particles fulfil this condition ([35]). A DFT can be applied to the discrete signal $r_i(\theta_i)$, and will provide the discrete Fourier spectrum $\{A_n, B_n\}$ of this signal, such that:

$$A_n = \frac{1}{N} \sum_{i=1}^{N} [r_i \cos(i \cdot \theta_i)] \tag{6}$$

$$B_n = \frac{1}{N} \sum_{i=1}^{N} [r_i \sin(i \cdot \theta_i)] \tag{7}$$

The average radius of the particle r_0 is given by:

$$r_0 = \frac{1}{N} \sum_{i=1}^{N} [r_i] \tag{8}$$

Thus, the number N of harmonics is equal to the number of points used to discretize the particle contour. Practically, it is convenient to use the classical fast Fourier transform (FFT) algorithm, which is commonly available in most commercial processing tools such as Matlab, to compute the DFT of the signal. The FFT requires that the number of points (and thus of harmonics) should be equal to a power of 2 in order for it to be efficient. Following [36], only the modes of order running from 1 to $N/2$ are kept in the spectrum as the remaining terms correspond to harmonics with a higher frequency than the one used for the sampling. A total of 128 points have been chosen in the present study, which leads to 64 effective harmonics.

In practice, such operations as particle microscope-scanning, image treatment, contour discretization and spectrum computation can be automated, as explained in [36]. In 2D, the images correspond to the orthogonal projections of the actual particle shapes. A more complete study in 3D might require some complex tools such as X-ray scanner or μ-CT. It has been shown in [34] and [36] that the normalized amplitude of the spectrum obtained by DFT is a relevant signature for a given population of granular particles with common shape properties. This normalized amplitude is given for each harmonic n by:

$$D_n = \frac{\sqrt{A_n^2 + B_n^2}}{r_0} \tag{9}$$

The amplitudes $\{D_n\}$ are called "Fourier descriptors". A typical normalized amplitude spectrum is provided in Fig. 2. The first Fourier descriptor D_0 is equal to 1 due to the normalization, since $\sqrt{A_n^2 + B_n^2} = r_0$. D_1 corresponds to a "shift" of the grain contour with respect to the position of point O, and can be set to zero if this point O is chosen properly. It is thus less relevant for the shape description. In contrast, D_2 is an extremely important descriptor, since it describes the elongation of the particle. As suggested in [36], the descriptors D_3 to D_8 can be regarded to define the main irregularities of the particle contour, and the modes D_n for $n > 8$ are good descriptors of the roughness of the particle surface. For natural sands, for example, it has been shown in [45] that these modes decrease linearly with the descriptor number in a log-log scale. The surface roughness of given sand can thus be described by only a slope and an intercept. In order to simplify the analysis, simple spectra will be defined hereafter using only the values of D_2, D_3, and D_8. The remaining descriptors will be assumed to follow the following expressions:

$$D_n = 2^{\alpha \cdot \log_2(n/3) + \log_2(D_3)} \quad \text{for } 3 < n < 8 \tag{10}$$
$$D_n = 2^{\beta \cdot \log_2(n/8) + \log_2(D_8)} \quad \text{for } n > 8 \tag{11}$$

Equation (11) is consistent with the observations of [45], i.e. the amplitudes of the modes larger than 8 decrease linearly with n in a $\log_2 - \log_2$ scale, with a slope β. Likewise, Eq. (10) is proposed for the modes 4–7, except that the slope is equal to α. In the present study, we adopt that:

$$\alpha = \beta = -2 \tag{12}$$

Such simple spectra are only chosen here for illustrative purpose, to ease the parametric studies by controlling them with
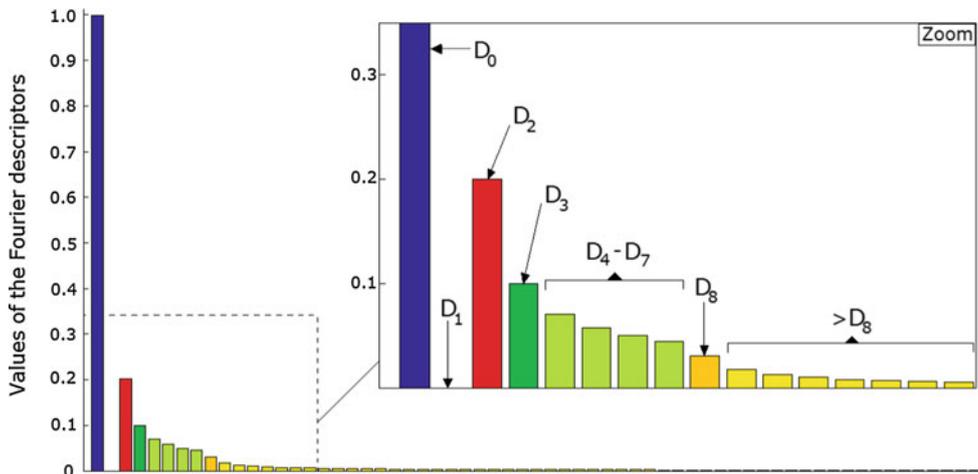

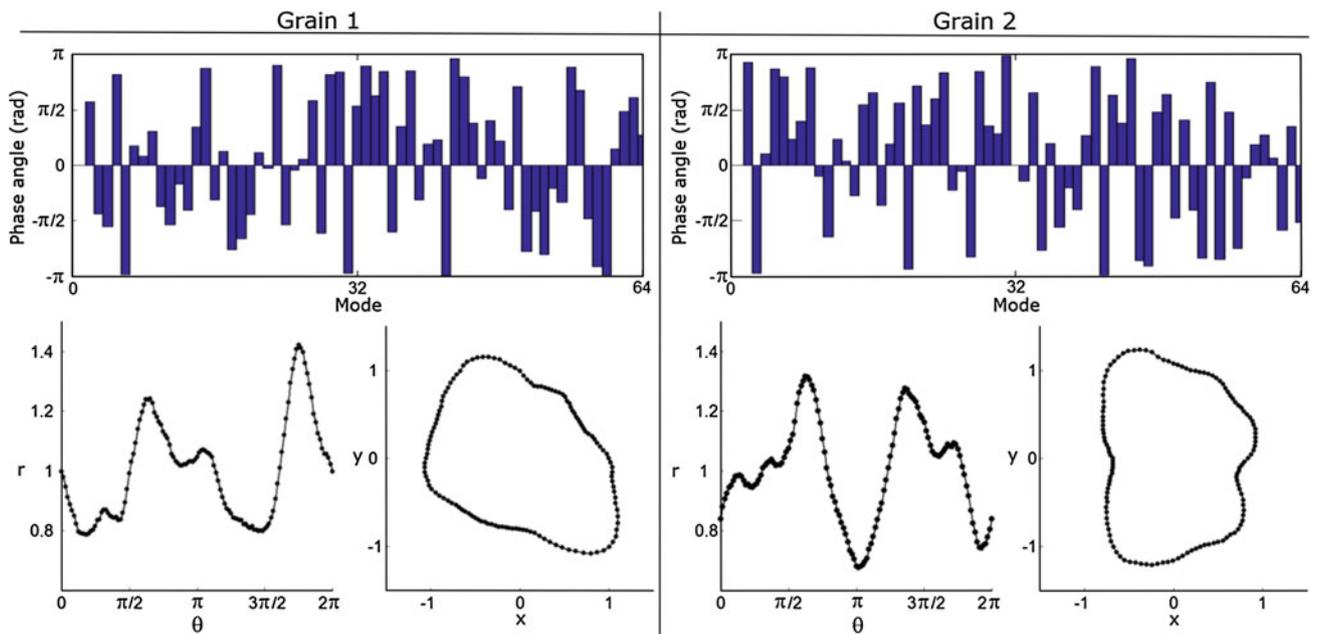**Fig. 2** Illustrative normalized amplitude spectrum

Fig. 3 Example of random generation of two grains with the illustrative spectrum of Fig. 2: random sampling of the phase angles, computation of the random signals $r(\theta)$, plotting of the corresponding particles contours

only 3 parameters. Apparently, using more accurate spectra according to Eqs. (5)–(9) may lead to high confidence in reproducing the shape of a real material.

2.3 Grain generation method

As a method to characterize the shape of a particle or of a population of particles, the Fourier descriptors may also be used to perform the reverse operation, i.e. to generate a particle with prescribed features. A large number of particles with different size can share the same amplitude spectrum and meanwhile have different shapes, as long as the main features of these shapes are similar. Thus, to generate a relevant and realistic population of particles with different shapes but with the same amplitude spectrum, some randomness needs to be introduced in the process. This can be done by considering the phase angle δ_n of each mode of amplitude D_n. For a given particle, these phase angles are defined by:

$$\delta_n = \tan^{-1}\left(\frac{B_n}{A_n}\right) \tag{13}$$

Thus, a random particle with a prescribed amplitude spectrum $\{D_n\}$ can be generated by randomly assigning a phase angle δ_n to each mode of order greater than zero. Each of these random angles follows a uniform distribution on the interval $[-\pi; \pi]$. The discretized contour of the considered particle is obtained using Eq. (5), with:

$$A_n = D_n \cdot \cos \delta_n \tag{14}$$

$$B_n = D_n \cdot \sin \delta_n \tag{15}$$

The present study adopts this method to generate particles. Two examples of grain generations are presented in Fig. 3, each of which follows the amplitude spectrum provided in Fig. 2. It is clear from the figure that the random phase angles lead to different $r_i(\theta_i)$ signals and different grain shapes, but with common features which are easily identifiable (e.g. the amplitude and the frequency of the irregularities and the particle aspect ratio).

The influence of the Fourier descriptors based on Eqs. (10) and (11) is demonstrated in Figs. 4 and 5. Figure 4 presents nine randomly generated particles at different D_2 and D_3 with D_8 fixed at zero. Evidently, for $D_2 = D_3 = 0$, the particle is a perfect disk. An increase in D_2 tends to enhance the elongation of the particle, while an increase of D_3 [and subsequently increases of D_4 to D_7 which are linked to D_3 through Eq. (10)] tends to add irregularity to the particle contour. Presented in Fig. 5 are the particles generated by fixing $D_2 = D_3 = 0$ and varying the value of D_8. It clearly shows that an increase of D_8 [and of the modes greater than $n = 8$, which are linked to D_8 by Eq. (11)] does not affect significantly the overall shape of the particle which remains roughly circular. Nevertheless, it does increase the roughness of the particle surface. It is evident from Figs. 4 and 5 that the three parameters D_2, D_3 and D_8 in conjunction with Eqs. (10) and
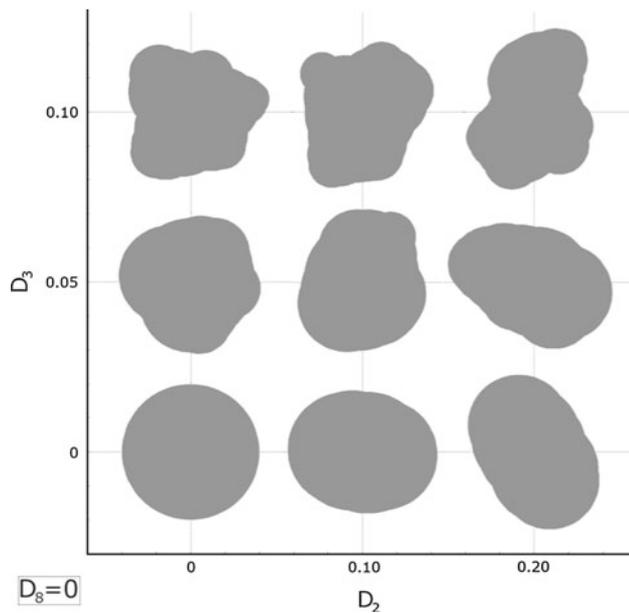
Fig. 4 Influence of the Fourier descriptors D_2 and D_3 on the shape of randomly generated grains
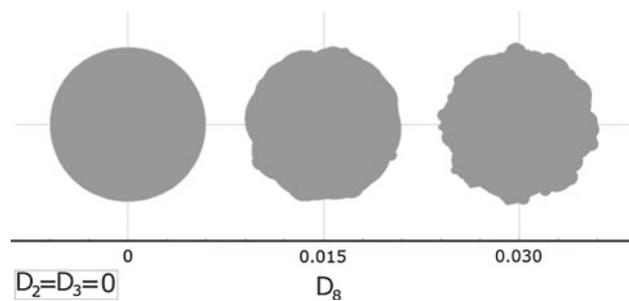

Fig. 5 Influence of the Fourier descriptor D_8 on the shape of randomly generated grains

(11) can provide a good control of the main features of the shape of the generated particle.

3 Constrained voronoi tessellation

3.1 Packing principles

The tools presented in the previous section make it possible to generate random population of particles with different shapes but with common normalized amplitude spectra. Before they can be used in a DEM simulation, the generated particles have to be appropriately packed. Importantly, it is desirable to generate the particles in a given domain, by following some conditions of grain size and orientation distributions as well as solid/void fraction.

The current study employs the Voronoi Tessellation [46] to divide a domain into small cells. For a given number of

seeding points P_i generated in the domain (they can be either randomly generated or specifically aligned), this Voronoi tessellation provides a set of polygons, one for each point in the domain. For a given polygon corresponding to the point P_i, the following condition is imposed: if and only if a point P of the space is located strictly inside the polygon, then $PP_i < PP_j, \forall j \neq i$. Thus, each polygon denotes a domain of points which are closer to P_i than to any other point P_j. Such a polygon is called a Voronoi cell. Voronoi tessellation has proved to be classical and efficient in defining the geometry of Voronoi cell for a given cloud of points. It is used in the present study to partition a domain for packing an assembly of particles, and each generated particle belongs to only one of the Voronoi cells.

Notably, however, the classical Voronoi tessellation has two obvious drawbacks to perform such an operation:

(a) Some of the Voronoi cells may be "open". Indeed, each Voronoi cell related to a point P_i is also defined as the intersection of a number of half-spaces (each one defining the points closer to P_i than to another point P_j), and this intersection may not be a closed domain if the point P_i lies on the border of the cloud of points.

(b) There is no direct method to generate a cloud of points P_i in such a way that their Voronoi cells follow the prescribed statistical distributions in terms of particle sizes and orientations.

Two algorithms are proposed to address the above issues. One is called the bounded Voronoi tessellation method and the other is the inverse Monte–Carlo (IMC) method. The performance of two methods will be compared by examples in later sections.

3.2 Bounded Voronoi tessellation

This subsection describes an algorithm to generate a closed Voronoi tessellation, i.e. a tessellation for which each of the seeding points P_i of the chosen domain D is assigned a closed cell, the union of all these cells being equal to D. As an example, let us consider the example provided in Fig. 6. In this example, 100 points (x_i, y_i) have been generated randomly in the square domain of the plane (x, y), such that $0 < x_i < 1$ and $0 < y_i < 1$ (Fig. 6a). The proposed algorithm of bounded Voronoi tessellation follows the subsequent steps:

(a) A classical Voronoi tessellation is performed (Fig. 6b).
(b) The "problematic" cells are identified (in red in Fig. 6c). A "problematic" cell refers to one that is not closed, or has at least one vertex outside of the domain D.
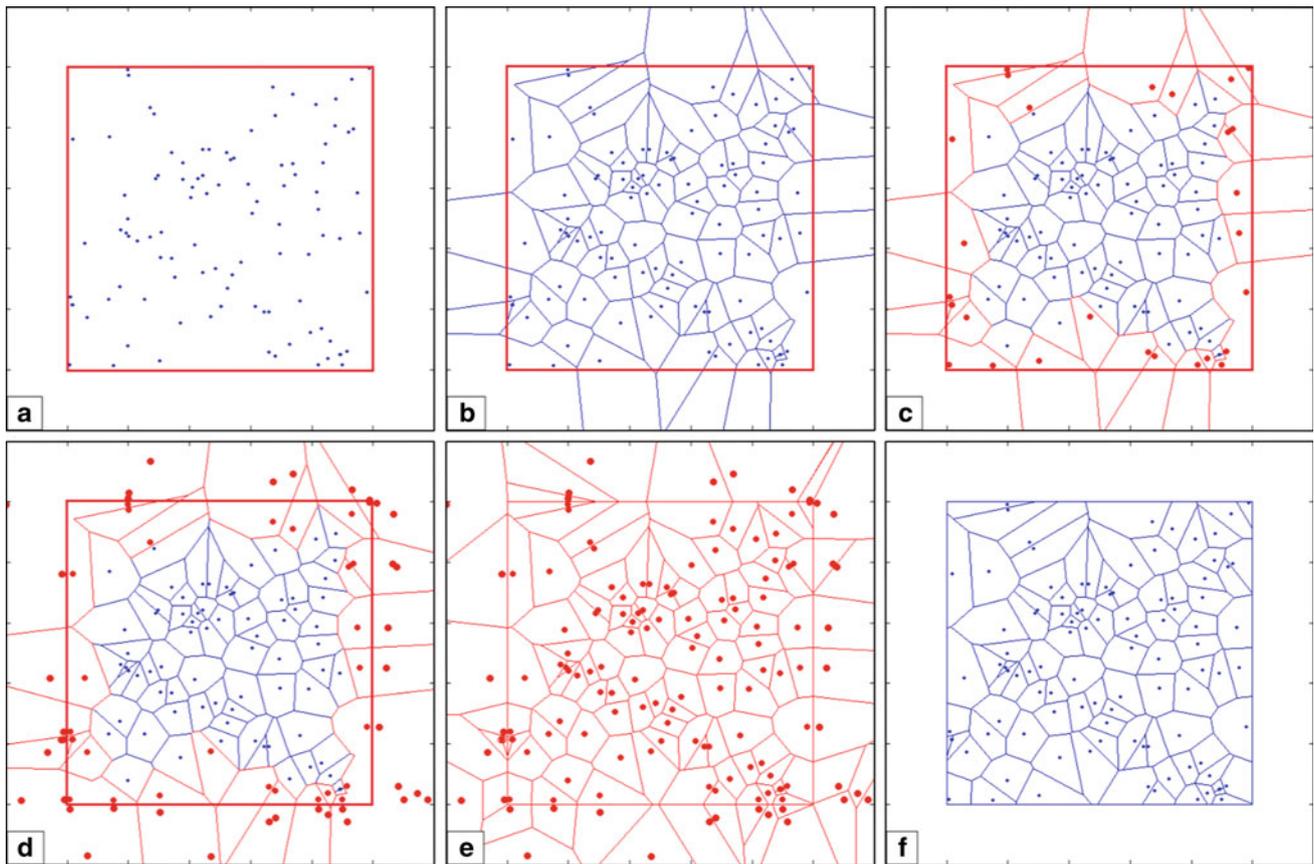(c) A number of new points are created outside of the domain D (Fig. 6d). These points are the symmetric

Fig. 6 Illustration of the stages of the bounded Voronoi tessellation algorithm

points to the problematic ones, with respect to the boundaries of D.

(d) A new classical Voronoi tessellation is performed (Fig. 6e), by considering both the initial cloud of points and the new points generated outside of the domain.

(e) From this new tessellation, only the cells corresponding to the initial points are kept.

As shown in Fig. 6f, after the above operation, there will be no more open or problematic cells, and the union of all these cells is equal to the target domain D. Indeed, key to this algorithm lies in closing the problematic cells by adding some half-spaces to their intersection-based definition.

3.3 Inverse Monte–Carlo (IMC) method

3.3.1 Main IMC algorithm

As mentioned before, the set of points generated in the domain should necessarily lead to a Voronoi tessellation with prescribed statistics in terms of cell size and orientations. Note that a method with prescribed elongation on the Voronoi cells has been described in [23]. It is not followed in

the present study since the final elongation of the particles is ensured by their Fourier spectrum, irrespective of the shape of the surrounding Voronoi cell. Thus, this section only deals with the size and orientation of the cells.

A method called IMC proposed in [37] and [38] may help us to generate points with such constraints. In essence, this stochastic iterative method introduces random modifications in a set of points to improve the statistics of the corresponding Voronoi tessellation as compared to the target distributions. The process is continued iteratively to render the set of points tending gradually to the desired distributions until certain prescribed tolerance is met. This method comprises of the following major steps [37]:

(a) Generate an initial set of points within the selected domain, and perform a Voronoi tessellation.

(b) Evaluate the statistics of this Voronoi tessellation (note that we are here focusing on the cells size and orientation distributions, but it could be any other properties, such as the number of neighbours or the perimeter).

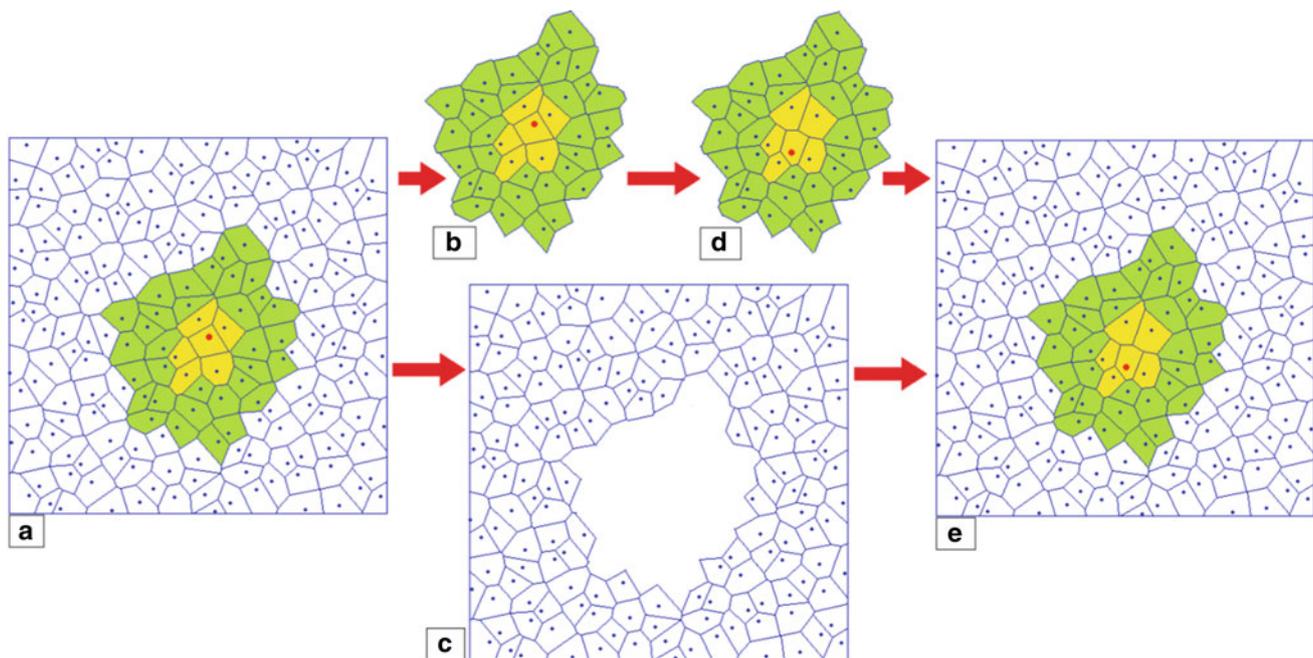(c) Compute an error corresponding to the discrepancy between the current and the target statistics.

Fig. 7 Illustration of the stages of the proposed improved IMC algorithm

(d) Move randomly one of the points of the set to another position in the domain. Compute the new Voronoi tessellation, and the new error value.

(e) If the error has been reduced with respect to the previous state, accept the modification. Otherwise, ignore it.

(f) Cycle on Steps (d) and (e) until the error is smaller than a prescribed threshold.

This algorithm has been found generally robust. However, it can become very slow and inefficient when dealing with a large sample, because it requires the computation of the whole Voronoi tessellation at each cycle. An improvement of the algorithm is herein proposed. Specifically, Step d) of the original IMC algorithm is replaced by the following operations, by only modifying the local cells around the moving point (see an illustrative case in Fig. 7):

(d1) Choose randomly one of the points (e.g. the red dot in Fig. 7a).

(d2) Define two sets of Voronoi cells: Set 1 corresponds to the initial Voronoi cell of the chosen point and all its immediate adjacent cells (yellow area in Fig. 7a); Set 2 corresponds to two more successive "layers" of cells around the Set 1 (green area in Fig. 7a).

(d3) Consider only these two sets of cells (Fig. 7b) and ignore the rest of the points (Fig. 7c).

(d4) Move the selected point randomly to a new position located somewhere in the first set of cells (yellow area).

Compute the new Voronoi tessellation of the union of the two sets of cells only (Fig. 7d).

(d5) Reintroduce the new Voronoi tessellation inside the existing one, and update the statistics of the global tessellation. Go on with Step e).

Though not particularly straightforward to implement, this new algorithm has the advantage to increase dramatically the computation speed, especially in the case of large samples. After this modification, the computation efficiency of each cycle of IMC has been found largely insensitive to the total number of points.

3.3.2 Convergence of the algorithm

The number of cycles necessary to obtain convergence depends on a number of factors: the chosen formulation of the error function, the threshold value of this error function, the number of Voronoi cells, the configuration of the initial set of points and the target distributions of the size and orientation of the Voronoi cells. It is instructive to carry out a brief sensitivity study on convergence here. To reduce the number of parameters of this study, the following assumptions are made (notice however that none of them is mandatory, and that different choices may be made in different contexts):

- The target distribution of the area S (considered here as a random variable) of the cells follows a lognormal law with a mean $\mu(S) = N_p/S_D$ (N_p being the number of Voronoi cells and S_D being the area of the domain) and
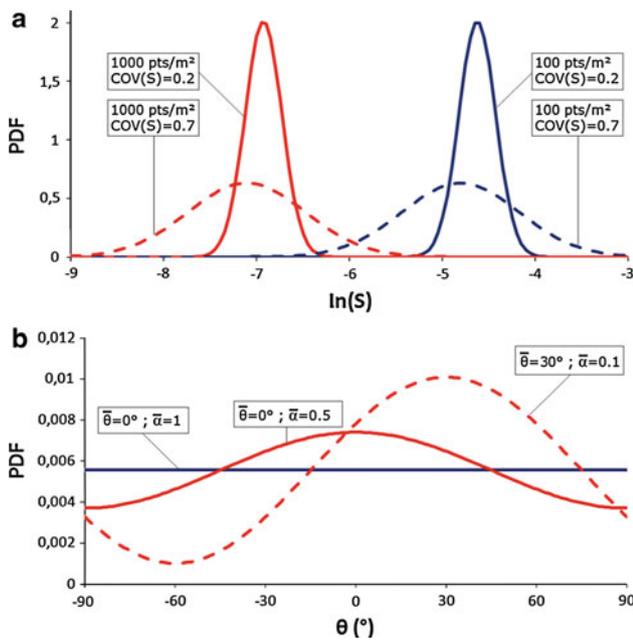
Fig. 8 Examples of target PDF: **a** cell areas; **b** cell orientation

Fig. 9 Typical sets of points and corresponding Voronoi cells: **a** uniform distribution; **b** Halton sequence

a standard deviation $\sigma(S) = COV(S) \cdot N_p/S_D$. Thus, when the domain and the number of cells have been defined, the size distribution is only dependent on one parameter, namely, the coefficient of variation $COV(S)$, which is equal to the ratio between the standard deviation and the mean value of the random variable S. As shown in the examples provided in Fig. 8a, the lognormal distribution of S corresponds to a normal distribution of $\ln(S)$. It should also be noted that a lognormal distribution has been chosen here to render the case as general as possible. More specific distributions or size parameters (such as the coefficient of uniformity commonly used in soil mechanics) may be easily dealt with in the general framework of this method.

- The target distribution of the cell orientation θ (this orientation being defined in the same way as for the particles, c.f. Fig. 1a) is proportional to a cosine of period π. It is defined by two parameters: the angle $\bar{\theta}$, corresponding to the maximum probability of occurrence, and the anisotropy ratio $\bar{\alpha}$, corresponding to the ratio between the minimum (for $\bar{\theta} \pm 90°$) and the maximum (for $\bar{\theta}$) probabilities of occurrence. Notice that this distribution is normalized in order for its integral on a π-period to be equal to 1. Figure 8b provides several examples with different values of $\bar{\theta}$ and $\bar{\alpha}$.
- The initial set of points used for the Voronoi tessellation may be defined in many ways. Two specific methods are chosen in this study and illustrated in Fig. 9. The first method is to generate the points with a classical pseudo-random number generator with a uniform distribution in
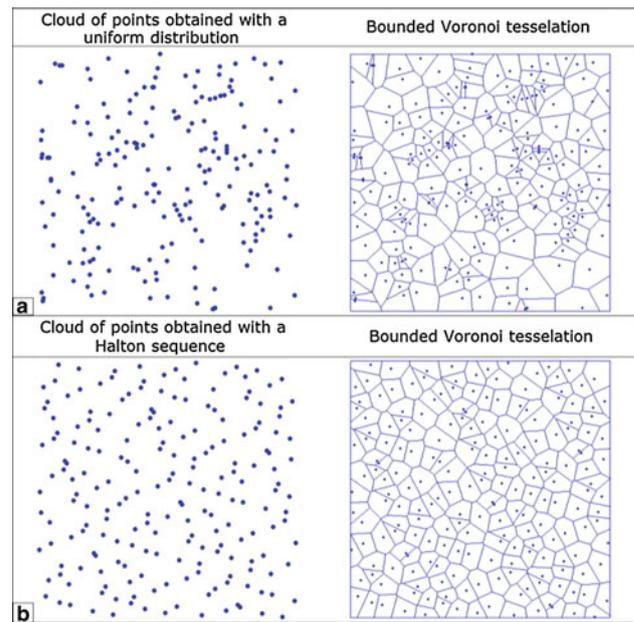
the domain. The second method employs a low-discrepancy algorithm, such as the Halton sequences [47]. As shown in Fig. 10, a uniform distribution leads to a great variety of sizes for the Voronoi cells, while a generation based on the Halton sequences leads to a set of cells with similar areas because this method has been designed to fill a domain of space as homogeneously as possible.

- Three different formulations are examined for the error function. They all express the discrepancy between the current statistics of the Voronoi tessellation and the target one, using the current and target normalized histograms (NH) of the size (respectively h_S and H_S) and orientation (respectively h_θ and H_θ) of the particles. These NH are obtained by dividing the histograms (i.e. the numbers of occurrences in each class corresponding to an interval of sizes or orientations) with the number N_p of Voronoi cells, in order for them to be independent of this number. The three error functions considered in this study are:

$$E_1 = 0.5 \left(\sqrt{\sum_i \left(h_{S,i} - H_{S,i} \right)^2} + \sqrt{\sum_j \left(h_{\theta,j} - H_{\theta,j} \right)^2} \right)$$
(16)

$$E_2 = \max \left(\max_i \left(\left| h_{S,i} - H_{S,i} \right| \right), \max_j \left(\left| h_{\theta,j} - H_{\theta,j} \right| \right) \right)$$
(17)

$$E_3 = \max \left(\sqrt{\sum_i \left(h_{S,i} - H_{S,i} \right)^2}, \sqrt{\sum_j \left(h_{\theta,j} - H_{\theta,j} \right)^2} \right)$$
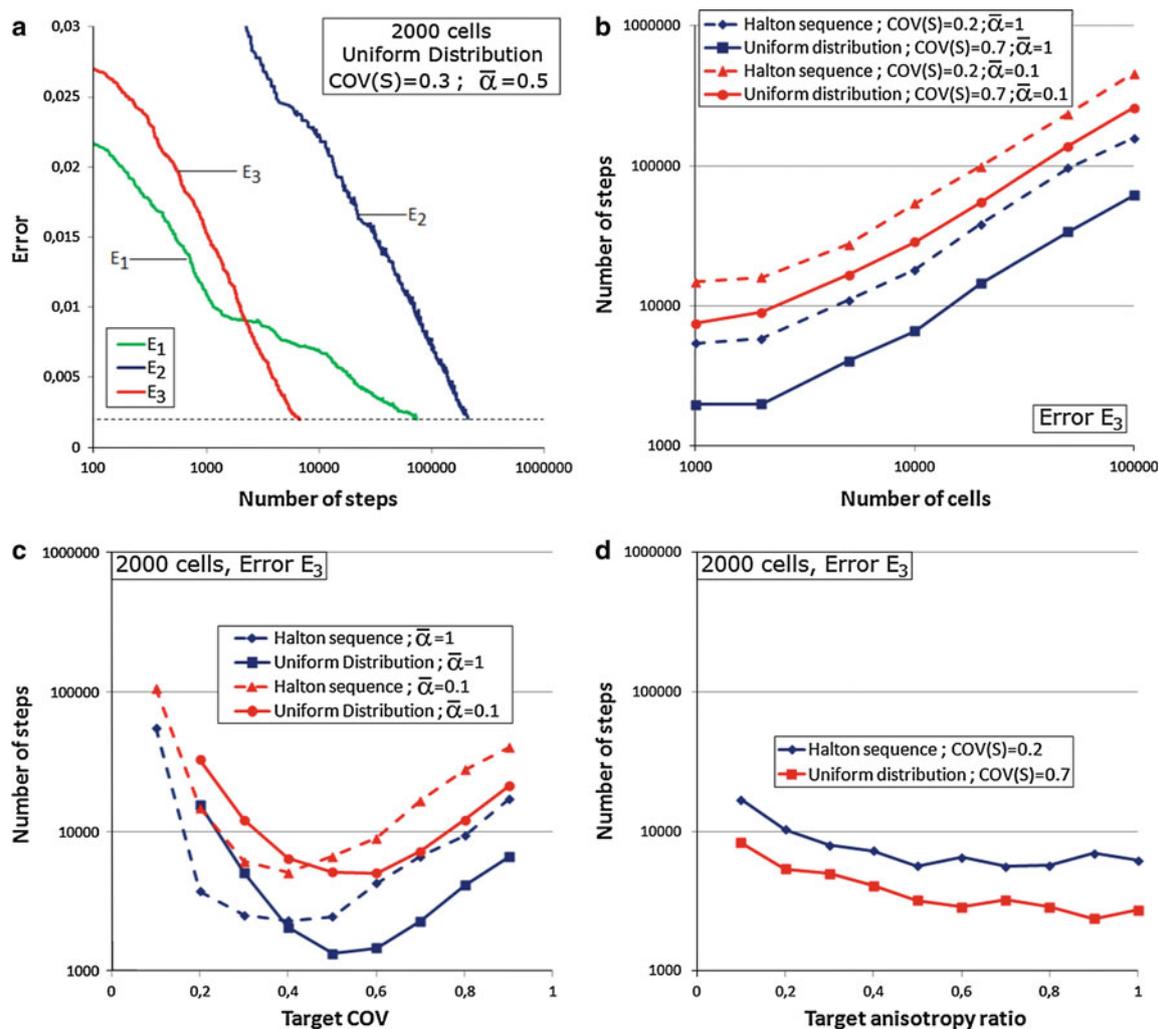(18)

Fig. 10 Convergence study of the IMC method: **a** influence of the error function formulation; **b** influence of the number of cells; **c** influence of the target COV(S); **d** influence of the target anisotropy ratio

Evidently, E_1 denotes the average between the mean square root errors of the size and orientation normalized histograms, E_2 is the maximum absolute difference on all the classes between the current and target normalized histograms (for both size and orientation), and E_3 is the maximum between the mean square root errors obtained on the sizes and orientations histograms. Figure 10a presents the evolution of these errors during IMC processes starting from the same initial configuration, in the case of 2,000 Voronoi cells. The number of steps on the horizontal axis of this chart corresponds to the number of displacements of any point of the set, may it be successful or not. Thanks to the improved IMC algorithm proposed earlier in this study, the computation time is directly proportional to this number of steps, but independent of the total number of points. Figure 10a clearly shows that the error E_3 leads to the best convergence rate. The error E_2 leads to a very slow rate of convergence, and the error E_1 is

inefficient as well. Moreover, E_1 may not be very satisfactory because it is the average between the errors on the size and on the orientation: it may thus lead to a very good configuration for one aspect and not good enough for the other. The error E_3 is thus more efficient and more relevant, and will be used in the rest of this article. The target threshold for which the IMC algorithm is considered to have converged is $E_3 = 0.002$.

Based on the above aspects, a convergence study is conducted and presented in Fig. 10b–d. Figure 10b shows the number of steps (i.e. the computation time) needed to reach $E_3 = 0.002$ with respect to the total number of points involved in the process. It clearly shows that, for N_p larger than 2,000, the computation time increases linearly with the sample size on a log-log chart. This observation is very interesting because it means that the method may be applied to very large samples at a reasonable computational cost. It

would not be the case without the improved IMC algorithm proposed earlier in the paper, because the cost of each cycle of the algorithm would be highly dependent on N_p.

Figure 10c shows the influence of the target value of $COV(S)$ on the number of steps needed for convergence. This figure shows that this parameter has a significant impact on the convergence rate, and that the method of generating the initial set of points should be chosen carefully. Indeed, an initial configuration based on a uniform distribution of the points leads to a faster convergence in the case of large values of $COV(S)$ (larger than 0.4), because the initial Voronoi cells already exhibit considerable size dispersion. On the other hand, when targeting small values of $COV(S)$ (i.e. smaller than 0.4), an initial configuration based on a Halton sequence helps to improve the convergence rate because the initial Voronoi cells have a relatively small dispersion. However, it is also found that the method could be computationally expansive in the case of very low and very high values of $COV(S)$ (i.e. lower than 0.1 or higher than 1). Figure 10d shows the influence of the target anisotropy ratio on the computational cost of the method. It appears that this parameter is much less critical than the size dispersion, although a small anisotropy ($\bar{\alpha} < 0.4$) might slightly increase the number of steps needed to reach convergence.

The improved IMC algorithm has been implemented in a Matlab environment (version 7.0) using one of the 8 cores of an Intel I7-2630QM CPU (2.0 GHz). The average computational time is close to 12 steps per second, and is independent of the total number of cells. In conjunction with Fig. 10, it is possible to estimate the computation time needed to reach convergence for a given configuration.

3.3.3 Examples

To illustrate the use of the IMC methodology in the framework presented in the previous subsection, two examples of target configurations with 500 cells in a unit square domain (i.e. $0 < x < 1$ and $0 < y < 1$) are presented. The target properties are:

- Configuration 1: $COV(S) = 0.8$; $\bar{\alpha} = 1$
- Configuration 2: $COV(S) = 0.2$; $\bar{\alpha} = 0.1$; $\bar{\theta} = 0°$

Figure 11 presents (from left to right) the initial configuration, the result for target configuration 1, and the result for target configuration 2. For each case, it provides (from top to bottom) the size distribution (target and obtained), a plot of the cells with colours corresponding to sizes, the orientation distribution (target and obtained), and a plot of the cells with colours corresponding to orientations. The match in terms of statistical distributions appears to be very satisfying, and the main differences between the two target configurations can easily be observed on the coloured plots. Configuration 1

depicts clearly a larger size dispersion without preferred orientation, while the cells of Configuration 2 are largely homogeneous in size but are mostly orientated along the horizontal direction.

4 Cell filling

4.1 Method of optimized cell filling

The IMC method presented in the previous section makes it possible to partition a container-domain into a number of polygonal sub-domains with prescribed statistics in terms of size and orientation. Each of these cells may then be filled with a particle with required shape generated using the method presented in Sect. 2. Meanwhile, to take advantage of the prescribed properties of the Voronoi tessellation obtained by IMC, the particles should be able to reproduce the properties (size and orientation) of the cells in which they are generated. A method is proposed as follows to respect this condition when filling a polygonal cell with a particle with a given Fourier spectrum. For each particle, an optimization is performed such that this particle occupies a prescribed proportion of the polygonal cell and meanwhile is entirely contained inside the cell. This optimization is performed on seven variables: the phase angles of Modes D_2 to D_7 (i.e. the modes that are considered to control the particle shape, as proposed in Sect. 2), and the average radius r_0 of the particle. The particle shape is obtained from the following minimization, using the notations shown in Fig. 12:

$$\min_{r_0,\delta_2,\delta_3,\delta_4,\delta_5,\delta_6,\delta_7} \left(\frac{S_p}{S} - F_S \right)^2$$

$$\text{subjected to } r_i < r_{\max,i} \forall \theta_i \tag{19}$$

where F_s is the target solid fraction in the cell (i.e. the proportion of the area of the cell covered by the particle), S_p is the particle area, S is the cell area, and r_i and $r_{\max,i}$ are the radial distances from the centre to the edges of the particle and of the cell, respectively, for an angle θ_i with $1 \leq i \leq 128$. The set of variables $(r_0, \delta_2, \delta_3, \delta_4, \delta_5, \delta_6, \delta_7)$ obtained from this optimization is combined with the chosen discrete normalized amplitude spectrum $\{D_n\}$ and the random values for the remaining phase angles (δ_n for $n > 7$). The final contour of the particle is computed from Eqs. (14), (15), and (5). The example shown in Fig. 12 corresponds to a target solid fraction equal to 0.5, which is a relatively loose sample indeed. In this case, the optimization of Eq. (19) is very fast and does not lead to any problem. However, when targeting high values of solid fraction (e.g. 0.7 or higher), some difficulties may arise because of the condition $r_i < r_{\max,i} \forall \theta_i$, which might introduce local optimums and prevent it from reaching the target filling. A good way to overcome this issue
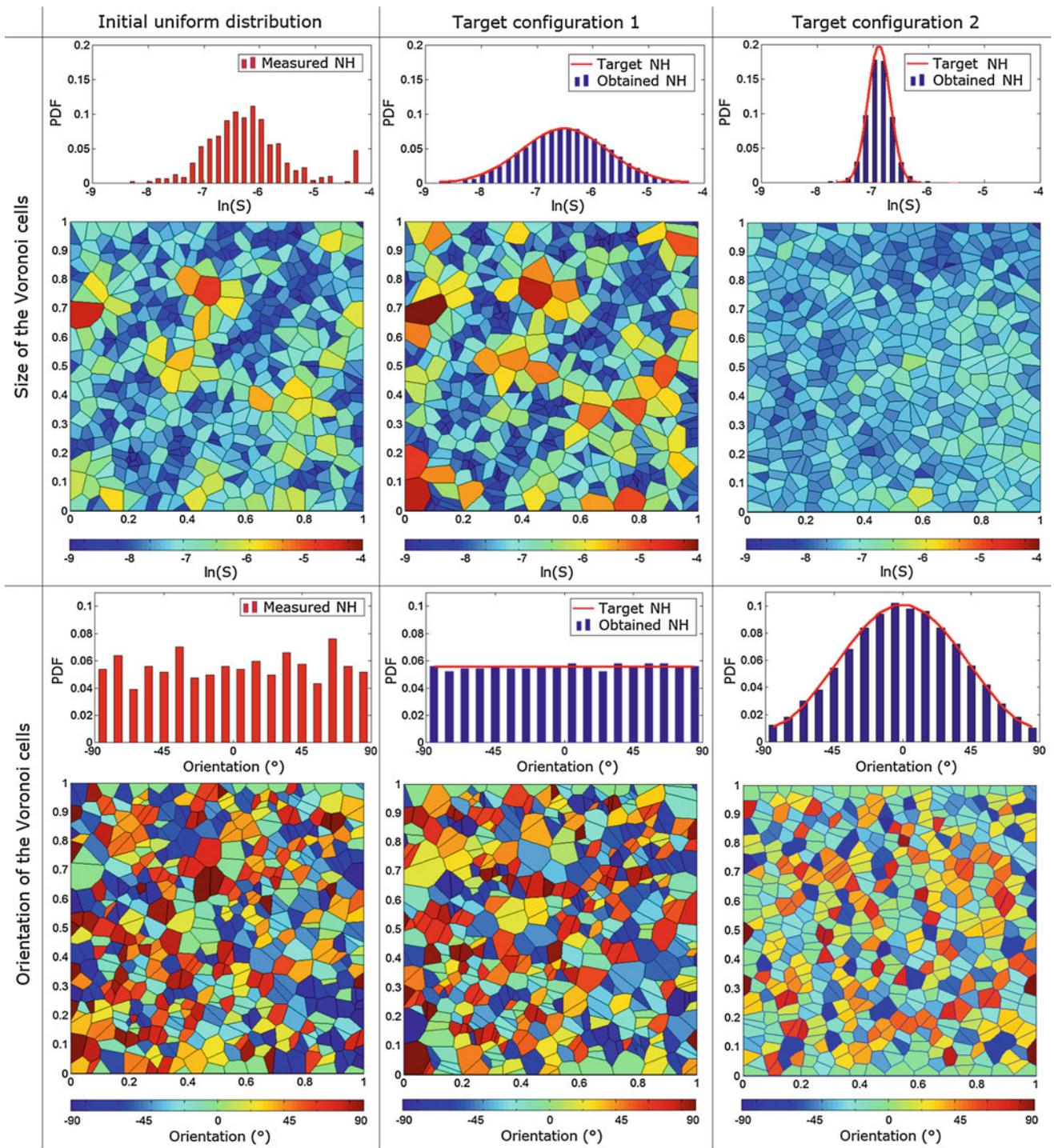
Fig. 11 Results of the IMC method on two illustrative target configurations

is to choose carefully the starting point of the optimization. It is suggested to choose the initial values of $\delta_n (2 \le n \le 7)$ and r_0 such that they are identical to the ones obtained after running a DFT on the contour of the polygonal cell. In this way, after the first trial of the optimization process, the shape and orientation of the tentative particle will be quite close to

those of the cell, and a filling with high solid fraction will be easier to achieve.

The cell-filling algorithm has been coded in Matlab, with a classical penalty method being used to deal with the constrained optimization of Eq. (19). One of the main features of this method is its high parallelizability. Indeed, as soon as
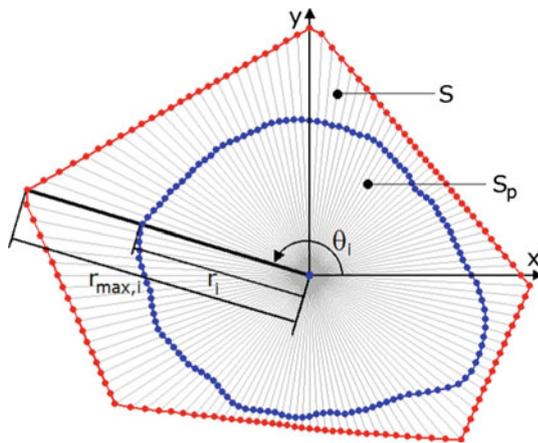
Fig. 12 Notations used in the cell-filling method

the IMC has provided a suitable Voronoi tessellation, all the cell-filling operations are perfectly independent and do not require any information exchange. This is the perfect configuration for multi-processing-unit computations and makes it applicable to large samples (although no parallelization has been coded in the current version of the algorithm). Using only one processor with Matlab, the current computation time of the cell-filling algorithm is close to 1 s per particle.

4.2 From contour to ODEC

The particle shape defined in previous subsection cannot be introduced directly in a DEM code because commonly available DEM codes are not able to perform neighbourhood and contact detections with arbitrary shapes. One of the most convenient methods to deal with this issue is to use the ODEC framework, as proposed in [40] and [41]. In this framework, the complex shape of a particle is filled with a collection of overlapping disks (spheres in 3D) which are rigidly assembled as a single "cluster". Such a cluster may then be introduced in a DEM code for neighbourhood and contact detections. This method is used in the remainder of this article, and the interested reader may find a detailed description of the ODEC algorithm in [40].

4.3 Shape descriptors versus Fourier descriptors

In order to investigate the relationship between the shape descriptors in Sect. 2.1 and the Fourier descriptors in Sect. 2.2 used to generate granular assemblies with the method proposed here, several packings have been performed and analysed. Each of these 75 packings involved 1,000 particles in a unit-square domain ($0 < x < 1$ and $0 < y < 1$), and used the spectra corresponding to all the combinations between the following Fourier descriptors:

- $D_2 = \{0; 0.05; 0.10; 0.15; 0.20\}$
- $D_3 = \{0; 0.025; 0.050; 0.075; 0.100\}$
- $D_8 = \{0; 0.015; 0.030\}$

The descriptors D_4 to D_7 and the ones after D_8 have been obtained using Eqs. (10) and (11), respectively. A target value $F_s = 1$ has been chosen during the particle generations [see Eq. (19)] in order to maximize the packing density. Each particle is then filled by overlapping discs using the ODEC method, so that all the shape descriptors computed hereafter correspond to the actual shapes of the particles as they would be introduced in a DEM code. For each packing, the mean values of elongation, roundness, circularity and regularity of the 1,000 particles are computed. The results are presented in Fig. 13. As can be seen from the figure, the average elongation is largely influenced by Mode D_2 only. All the other modes hardly have an effect on this descriptor. A quite different behaviour is observed for the roundness: for "smooth" particles (i.e. particles for which $D_n = 0$ for $n > 7$), the roundness seems to be only affected by the modes D_3 to D_7. However, once certain surface roughness is introduced, the influence of the modes D_3 to D_7 become much less significant, and D_8 and other greater modes tend to dominate the behaviour of the roundness.

The circularity of the particles seems to be rather independent on Mode D_8 and larger ones, which is somehow expected since this descriptor is mostly concerned with the overall shape of the particle rather than with the small irregularities of the surface. Thus, circularity appears to be strongly dependant on D_2 (because of the effect of this mode on the particle elongation, which unavoidably influences circularity) and on the modes D_3 to D_7 (which control the global shape of the particle). The last descriptor used in this study, the regularity, seems to have a somehow similar behaviour as the roundness. It correlates weakly with Mode D_2, but all the larger modes seem to influence it strongly. The regularity can be used together with the elongation as a global criterion for all the irregularities introduced by the normalized spectrum. It remains unclear how well each of the four descriptors may be able to predict the behaviour of a granular mass, and it is expected to be problem-dependant. The regularity introduced in this paper may be a good description of the shape irregularities at all scales, but it may also be "too general". Only a complete parametric study (focusing on a given problem) could bring an answer to this question, and it will be the topic of our future studies.

Figure 13 may be used as a reference to estimate the shape descriptors expected for a packing prepared by the proposed method. It may also be used to choose the descriptors D_2, D_3 and D_8 [jointly with Eqs. (10) and (11)] prior to such packing to match some target descriptors. For example, one may first choose D_2 to match some target average elongation (using the first row of Fig. 13), then choose D_3 to match some target
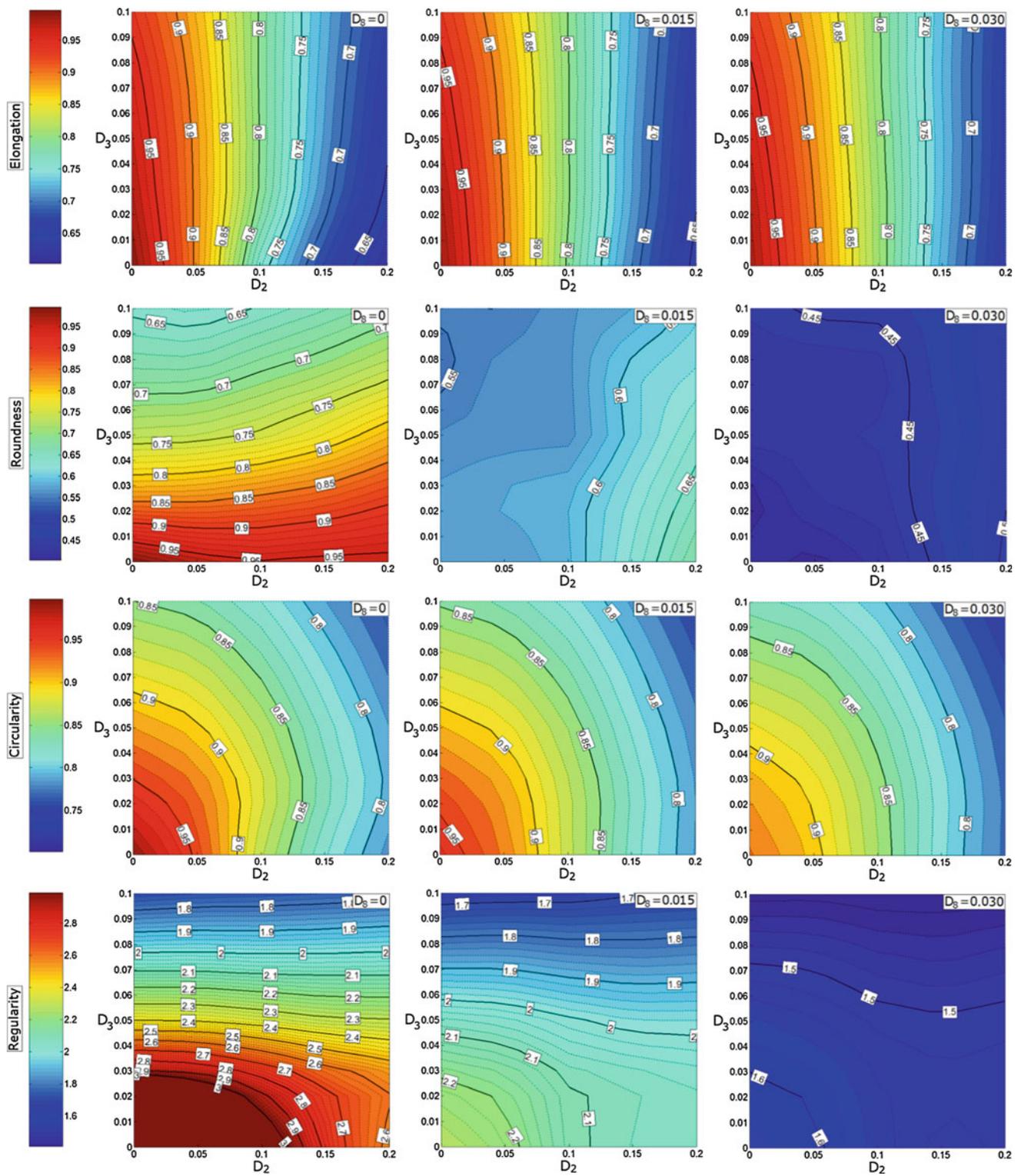
Fig. 13 Mean values of the shape descriptors of a particle (elongation, roundness, circularity and regularity) in relation with its Fourier descriptors
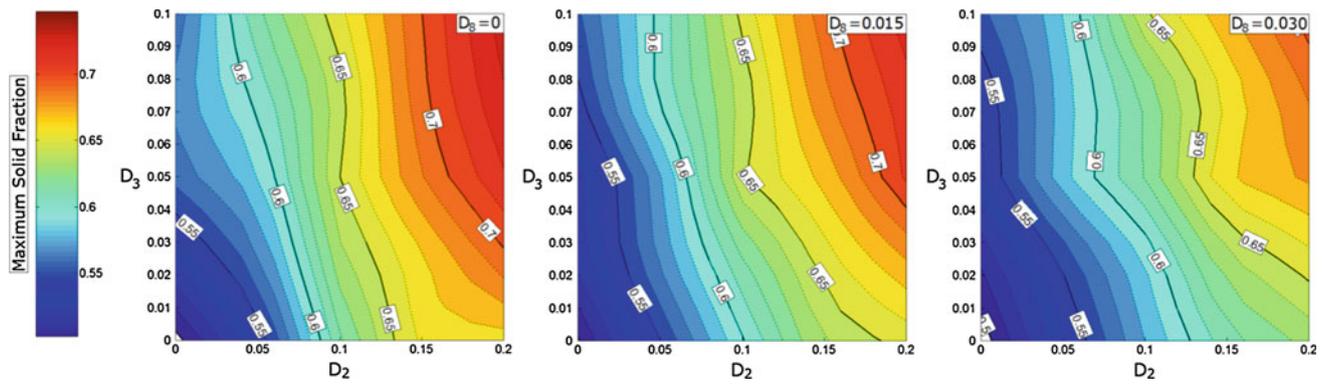
Fig. 14 Maximum solid fraction provided by the method with respect to the Fourier descriptors

circularity (using the third row of Fig. 13 with a fixed value of D_2), and then choose D_8 to match some target roundness or regularity.

Further presented in Fig. 14 is the maximum solid fraction that is achievable in a packing with respect to the values of D_2, D_3 and D_8 (this maximum solid fraction is the largest one that may be provided by this packing method, but not necessarily the largest density that the granular material may reach after compression). The figure indicates that this maximum density is strongly related to D_2, i.e., elongated particles are more likely to provide a good fill of the Voronoi cells (up to a solid fraction close to 0.72) while more rounded particles can hardly reach a density more than 0.55. It also shows that large values of D_3 may help to increase the maximum density (because they provide more freedom in the particle shape and thus make it easier to fill the Voronoi cell), while large values of D_8 might lead to slightly reduced maximum solid fraction.

5 Examples and discussion

Two packings of particles are generated to illustrate the potential of the proposed method. They make use of the illustrative Voronoi tessellations described in earlier sections as well as in Fig. 11. These rather dense packings are composed of 500 particles each, with the following distinctive features:

- Example 1: large size dispersion ($COV(S_p) = 0.8$), isotropic orientations ($\bar{\alpha} = 1$), moderate elongation, low roundness and regularity.
- Example 2: small size dispersion ($COV(S_p) = 0.2$), mostly horizontal orientations ($\bar{\alpha} = 0.1$; $\bar{\theta} = 0°$), elongated particles with high roundness and regularity.

The properties of size dispersion and orientation are directly obtained from the characteristics of the Voronoi tessellations described in Sect. 3, while the properties related to the shape

descriptors are obtained by choosing carefully the discrete Fourier spectrum. The target solid fraction is set to 0.65 in both examples. The Fourier descriptors and resulting solid fractions are presented in Fig. 15, along with the obtained packings. For each example, Fig. 15 provides a detailed view of the packing (Fig. 15a), two plots of the packing in which the coloured particles correspond to sizes (Fig. 15b) and orientations (Fig. 15c), the target and obtained size distributions (Fig. 15d), the target and obtained rose diagrams of the particles orientations (Fig. 15e), and the expected average values and obtained distributions of the four shape descriptors (elongation, roundness, circularity and regularity) (Fig. 15f–i). All these results show a fairly good match between the target and the realized statistics of the packings. It is evident from the examples that the proposed method is capable of generating a wide range of granular materials in very diverse configurations. A direct comparison between the packings (Fig. 15a) and the original Voronoi Tessellations (Fig. 11) shows that the algorithm of cell filling proposed in Sect. 4 leads to a very good correspondence between the statistics of each cell and of its filling particle, in terms of both size and orientation. The differences between the two packings in Fig. 15a are clearly recognizable: Example 1 reproduces an isotropic packing of irregular particles with very diverse size, while Example 2 corresponds to an anisotropic packing (mostly horizontal) of elongated but rather regular particles. The grain shapes and sizes of the first example are somehow similar to the ones of real sand, while those of the second example are more often encountered in industrial powder processes.

The solid fractions obtained in these two examples are quite similar ($F_s = 0.635$ and 0.623, which correspond, respectively to void ratios equal to 0.575 and 0.605, for the two examples) and both correspond to dense packings. Note however that the resulting solid fractions of the packings are slightly smaller than the target value ($F_s = 0.65$ in this case). This is because some cells of the Voronoi tessellation cannot be filled with the prescribed fraction, and this happens frequently with very elongated Voronoi cells.
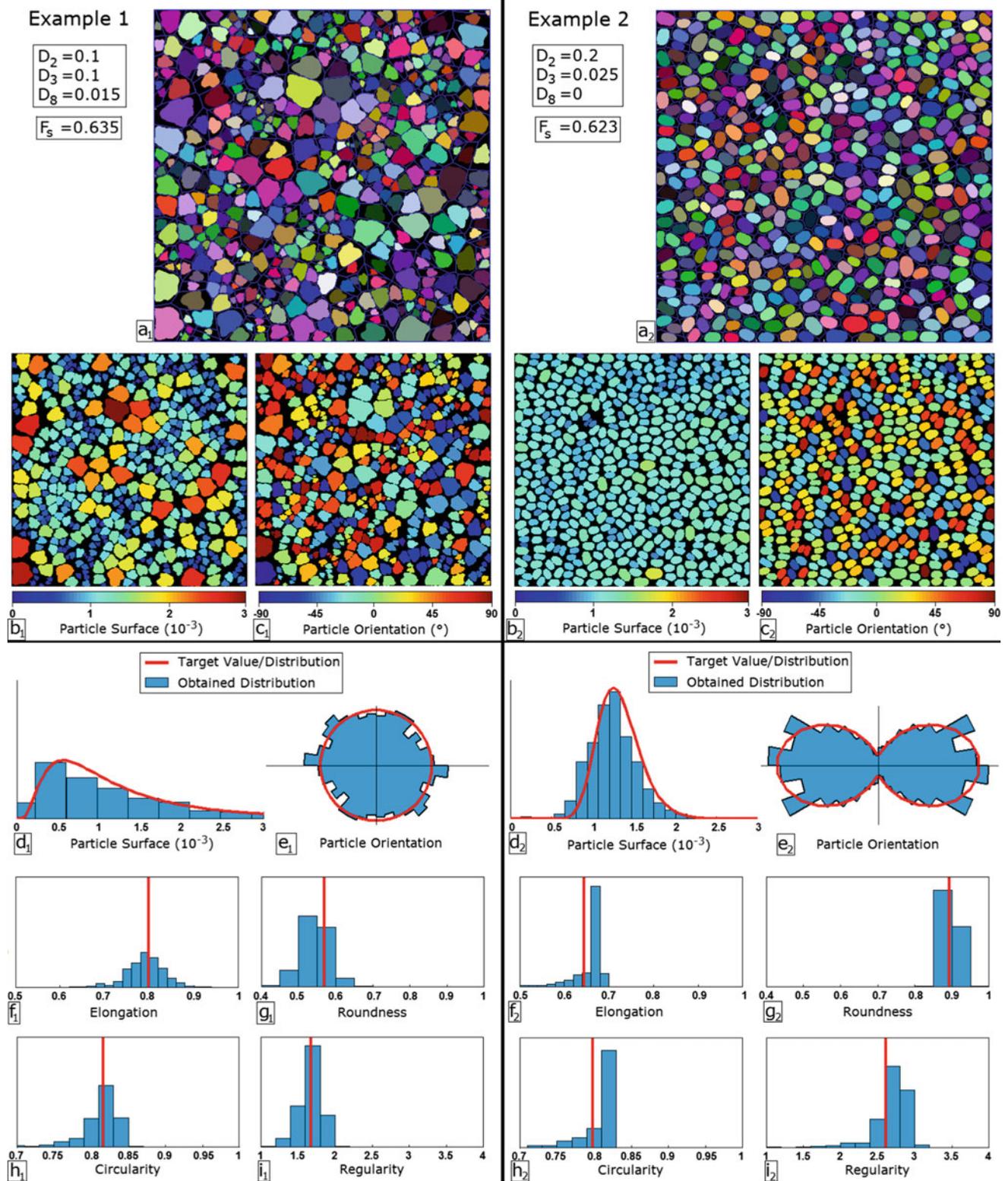
Fig. 15 Two detailed examples of packing: (a_1, a_2) detailed view of the packing; (b_1, b_2) particle sizes; (c_1, c_2) particle orientations; (d_1, d_2) target and obtained size distributions; (e_1, e_2) rose diagram of the target and obtained orientation distributions; (f_1, f_2) target value and obtained distribution of elongation; (g_1, g_2) target value and obtained distribution of roundness; (h_1, h_2) target value and obtained distribution of circularity; (i_1, i_2) target value and obtained distribution of regularity

Consequently, the resulting size distribution is always slightly shifted towards the left (smaller values) when compared to the target ones in both examples. In practice, it is suggested to prescribe a slightly larger density than the one which is actually desired. However, it is important to note that the solid fractions obtained by this packing method are not related to any stress state. The density will easily be changed with such processes as directional or isotropic compression and shear. The target density is hence not a key parameter of the method. It would be more appropriate to target a moderate value of solid fraction (when compared to the maximum one provided in Fig. 14) which corresponds to a medium dense case. This will facilitate the algorithm to fill the Voronoi cells accordingly to the prescribed density, and the size distribution will not be strongly disturbed. The desired void ratio might then be obtained later in the DEM code by applying gravity or isotropic pressure.

6 Conclusion

This article presents a new method for the generation and packing of samples of granular materials. Compared to existing methods, this new framework has the advantage to be capable of dealing with complex particle shapes and anisotropic particle orientations, in arbitrary container geometry. The proposed method features the following major steps (1) to generate a Constrained Voronoi Tessellation of the container with a number of polygonal subdomains by imposing the constraints of target statistics in terms of grain size and orientation, and (2) to fill each of these subdomains with a virtual particle respecting some target shape characteristics. To achieve the first goal, an existing stochastic and iterative method called IMC method initially proposed in [37,38] has been improved, implemented and fully tested, with much attention being paid to the accuracy and computational efficiency of the algorithm. A new method of random particle generation, inspired by the shape characterization methods proposed in [34–36] and based on the Fourier Descriptors approach with further improvement on filling each Voronoi cell efficiently, has been developed to fulfil the second goal. With two demonstrative examples, the proposed packing method proves to be capable of generating a wide range of granular samples, with greatly varied characteristics in terms of container shape, particle number, size distribution, particles orientations, elongations, and shapes and packing density. Indeed, there have been experimental data in geomechanics available on these properties (such as the Fourier amplitude spectra provided in [32] for several sands), which make it easy to apply this method directly to the modelling of real materials. In using the proposed method, however, extensive experimental benchmarking tests are still required to calibrate relevant parameters governing the contact behaviour of these materials. The proposed tool will also be useful to evaluate the influence of a number of key parameters (such as particles shapes and roughness, fabric anisotropy, size distribution) on the behaviour of granular materials subjected to different loading conditions (compression, shearing, flow, etc.), which will be the subjects of future studies.

The 2D formulation of the proposed method may seemingly limit its practical use for real 3D particle modelling. However, as far as we can see, there are no technical difficulties preventing the method being extended to a general 3D case, although the practical implementation of the algorithms for the 3D case may demand more effort. In generalizing the current methodology to the 3D case, addition shape descriptors, such as the flatness and angularity of a particle as defined in [5], may be further introduced. The Fourier spectra method and the Voronoi tessellation approach can be readily extended to 3D as well. Nevertheless, a major issue to be addressed would probably be the lack of experimental data for the calibration of 3D Fourier spectra of real materials. With the latest applications of such advanced technologies as high-definition micro-CT and X-ray to particle shape studies, this issue is more likely to be solved very soon. Therefore, it is expected the methodology and numerical tools developed in this paper may indeed open a wide range of interesting areas for realistic discrete modelling of granular materials.

References

1. Desrues, J., Viggiani, G.: Strain localization in sand: an overview of the experimental results obtained in Grenoble using stereophotogrammetry. Int. J. Numer. Anal. Methods Geomech. **28**(4), 279–321 (2001)
2. Hall, S.A., Bornert, M., Desrues, J., Pannier, Y., Lenoir, N., Viggiani, G., Béuelle, P.: Discrete and continuum analysis of localised deformation in sand using X-ray μCT and volumetric digital image correlation. Géotechnique **60**(5), 315–322 (2010)
3. Cavaretta, I., Coop, M., O'Sullivan, C.: The influence of particle characteristics on the behavior of coarse grained soils. Géotechnique **60**(6), 413–423 (2010)
4. Cundall, P.A., Strack, O.D.L.: A discrete numerical model for granular assemblies. Geotechnique **29**, 47–65 (1979)
5. Blott, S.J., Pye, K.: Particle shape: a review and new methods of characterization and classification. Sedimentology **55**, 31–63 (2008)
6. Cho, G., Dodds, J., Santamarina, J.C.: Particle shape effects on packing density, stiffness, and strength: natural and crushed sands. J. Geotech. Geoenviron. Eng. **132**(5), 591–602 (2006)
7. Jiang, M.J., Yu, H.-S., Harris, D.: A novel discrete model for granular material incorporating rolling resistance. Comput. Geotech. **32**(5), 340–357 (2005)
8. Thomas, P.A., Bray, J.D.: Capturing nonspherical shape of granular media with disk clusters. J. Geotech. Geoenviron. Eng. **125**, 169–178 (1999)
9. Jensen, R.P., Edil, T.B., Bosscher, P.J., Plesha, M.E., Ben Kahla, N.: Effect of particle shape on interface behavior of DEM-simulated granular materials. Int. J. Geomech. **1**(1), 1–19 (2011)

10. Salot, C., Gotteland, P., Villard, P.: Influence of relative density on granular materials behavior: DEM simulation of triaxial tests. Granul. Matter **11**, 221–236 (2009)
11. Stahl, M., Konietzky, H.: Discrete element simulation of ballast and gravel under special consideration of grain-shape, grain-size and relative density. Granul. Matter **13**, 417–428 (2011)
12. Katagiri, J., Matsushima, T., Yamada, Y.: Simple shear simulation of 3D irregularly-shaped particles by image-based DEM. Granul. Matter **12**, 491–497 (2010)
13. Matsushima, T., Katagiri, J., Uesugi, K., Tsuchiyama, A., Nakano, T.: 3D shape characterization and image-based DEM simulation of the Lunar soil simulant FJS-1. J. Aerosp. Eng. **22**(1), 15–23 (2009)
14. McDowel, G., Li, H., Lowndes, I.: The importance of particle shape in discrete-element modelling of particle flow in a chute. Géotech. Lett. **1**(3), 59–64 (2011)
15. Ng, T.-T.: Particle shape effect on macro- and micro-behavior of monodisperse ellipsoids. Int. J. Numer. Anal. Methods Geomech. **33**, 511–527 (2009)
16. Ouadfel, H., Rothenburg, L.: "Stress-force fabric" relationship for assemblies of ellipsoids. Mech. Mater. **33**, 201–221 (2001)
17. Lin, X., Ng, T.T.: A three-dimensional discrete element model using arrays of ellipsoids. Géotechnique **47**(2), 319–329 (1997)
18. Azema, E., Radjai, F., Peyroux, R., Saussine, G.: Force transmission in a packing of pentagonal particles. Phys. Rev. E **76**, 011301 (2007)
19. Azema, E., Radjai, F.: Stress-strain behavior and geometrical properties of packings of elongated particles. Phys. Rev. E. **81**, 051304 (2010)
20. Fu, P., Dafalias, Y.: Fabric evolution within shear bands of granular materials and its relation to critical state theory. Int. J. Numer. Anal. Methods Geomech. **35**(18), 1918–1948 (2011)
21. Pournin, L., Weber, M., Tsukahara, M., Ferrez, J.-A., Ramaioli, M., Liebling, Th.M.: Three-dimensional distinct element simulation of spherocylinder crystallization. Granul. Matter **7**(2–3), 119–126 (2005)
22. Azema, E., Radjai, F., Saussine, G.: Quasistatic rheology, force transmission and fabric properties of a packing of irregular polyhedral particles. Mech. Mater. **41**, 729–741 (2009)
23. Pena, A.A., Garcia-Rojo, R., Herrmann, H.J.: Influence of particle shape on sheared dense granular media. Granul. Matter **9**, 279–291 (2007)
24. Lu, M., McDowell, G.R.: The importance of modelling ballast particle shape in DEM. Granul. Matter **9**(1–2), 71–82 (2007)
25. Mollon, G., Richefeu, V., Daudon, D., Villard, P.: Assessment of DEM parameters for rock mass propagation. Second World Landslide Forum, 3–7 October 2011, Roma (2011) (in press)
26. Mollon, G., Richefeu, V., Villard, P., Daudon, D.: Numerical simulation of rock avalanches: influence of a local dissipative contact model on the collective behavior of granular flows. J. Geophys. Res. **117** (2012). doi:10.1029/2011JF002202
27. Tillemans, H.-J., Herrmann, H.-J.: Simulating deformations of granular solids under shear. Phys. A. **217**, 261–288 (1995)
28. Galindo-Torres, S.-A., Pedroso, D.-M.: Molecular dynamics simulations of complex-shaped particles using Voronoi-based spheropolyhedra. Phys. Rev. E. **81**, 061303 (2010)
29. Galindo-Torres, S.-A., Munoz, J.-D., Alonso-Marroquin, F.: Minkowski–Voronoi diagrams as a method to generate random packing of spheropolygons for the simulation of soils. Phys. Rev. E. **82**, 056713 (2010)
30. Houlsby, G.T.: Potential particles: a method for modelling non-circular particles in DEM. Comput. Geotech. **36**, 953–959 (2009)
31. Jerier, J.-F., Imbault, D., Donze, F.-V., Doremus, P.: A geometric algorithm based on tetrahedral meshes to generate a dense polydisperse sphere packing. Granul. Matter **11**, 43–52 (2009)
32. Bagi, K.: An algorithm to generate random dense arrangements for discrete element simulations of granular assemblies. Granul. Matter **7**, 31–43 (2005)
33. Sahu, K.K., Ishihara, K.N.: Modelling local voids using an irregular polyhedron based on natural neighbourhood and application to characterize near-dense random packing (DRP). Philos. Mag. **86**(36), 5909–5926 (2006)
34. Bowman, E.T., Soga, K., Drummond, W.: Particle shape characterization using Fourier descriptor analysis. Geotechnique **51**(6), 545–554 (2001)
35. Garboczi, E.J.: Three-dimensional mathematical analysis of particle shape using x-ray tomography and spherical harmonics: application to aggregates used in concrete. Cem. Concr. Res. **32**(10), 1621–1638 (2002)
36. Das, N.: Modeling three-dimensional shape of sand grains using discrete element method. PhD Thesis. University of South Florida. p 149 (2007)
37. Gross, D., Li, M.: Constructing microstructures of poly- and nanocrystalline materials for numerical modeling and simulation. Appl. Phys. Lett. **80**(5), 746–748 (2002)
38. Xu, T., Li, M.: Topological and statistical properties of a constrained Voronoi tessellation. Philos. Mag. **89**(4), 349–374 (2009)
39. Masad, E., Saadeh, S., Al-Rousan, T., Garboczi, E., Little, D.: Computations of particle surface characteristics using optical and X-ray CT images. Comput. Mater. Sci. **34**, 406–424 (2005)
40. Ferellec, J.-F., McDowell, G.R.: A simple method to create complex particle shapes for DEM. Geomech. Geoeng. **3**(3), 211–216 (2008)
41. Ferellec, J.-F., McDowell, G.: A method to model realistic particle shape and inertia in DEM. Granul. Matter **12**, 459–467 (2010)
42. Wadell, H.: Volume, shape, and roundness of rock particles. J. Geol. **40**, 443–451 (1932)
43. Riley, N.A.: Projection sphericity. J. Sed. Petrol. **11**, 94–97 (1941)
44. Ehrlich, R., Weinberg, B.: An exact method for characterization of grain shape. J. Sediment. Petrol. **40**(1), 205–212 (1970)
45. Meloy, T.P.: Fast Fourier transform applied to shape analysis of particle silhouettes to obtain morphological data. Powder Technol. **17**, 27–35 (1977)
46. Fortune, S.: A sweepline algorithm for Voronoi diagrams. Algorithmica **2**(1–4), 153–174 (1987)
47. Halton, J.: Algorithm 247: radical-inverse quasi-random point sequence. Com. ACM. **7**(12), 701 (1964)